(A New Proposal to Jefferson Lab PAC–30)

# *A Path to "Color Polarizabilities" in the Neutron: A Precision Measurement of the Neutron $g_2$ and $d_2$ at High $Q^2$ in Hall C*


S. Zhou and X. Li
*China Institute of Atomic Energy, Beijing 102413, P.R. China*

P. Markowitz
*Florida International University, Miami, FL 33199, USA*

A. Camsonne, J.-P. Chen, E. Chudakov, J.-O. Hansen, D.W. Higinbotham, M. Jones, A. Saha, B. Wojtsekhowski
*Jefferson Lab, Newport News, VA 23606, USA*

G.G. Petratos
*Kent State University, Kent, OH 44242*

W. Korsch (co-spokesperson)
*University of Kentucky, Lexington, KY 40506, USA*

K. Kumar, K. Paschke[1]
*University of Massachusetts Amherst, Amherst, MA 01003, USA*

W. Bertozzi, S. Gilad, X. Zheng[1]
*Massachusetts Institute of Technology, Cambridge, MA 02139, USA*

F.R. Wesselmann
*Norfolk State University, Norfolk, VA 23504, USA*

R. Gilman
*Rutgers University, Piscataway, NJ 08855, USA*

H. Lu, X. Yan and Y. Ye
University of Science and Technology of China, Hefei, Anhui 230026, P.R. China

Seonho Choi, Hyekoo Kang, Byungwuek Lee, Yumin Oh, Jongsog Song
*Seoul National University, Seoul 151-747, South Korea*

P. Souder
Syracuse University, Syracuse, NY 13244

A. Lukhanin, Z.-E. Meziani (co-spokesperson), B. Sawatzky (co-spokesperson)
*Temple University, Philadelphia, PA 19122, USA*

G. Cates, N. Liyanage, B. Norum, K. Slifer
*University of Virginia, Charlottesville, VA 22901, USA*

D. Armstrong, T. Averett (co-spokesperson), J. M. Finn, K. Griffioen, A. Kelleher, V. Sulkosky
*College of William and Mary, Williamsburg, VA 23185, USA*


July 7, 2006


Contact: Brad Sawatzky (brads@jlab.org)


[1] Affiliation starting September 2006: University of Virginia, Charlottesville, VA 22904

**Abstract**

We propose a precision measurement of the neutron spin structure function $g_2(x,Q^2)$ over the kinematic region $0.2 < x < 0.95$ and $2.5 < Q^2 < 6\mathrm{GeV}^2/c^2$. In addition to mapping out the $x$ and $Q^2$ evolution of $g_2^n$ which (in contrast to $g_1$) is poorly understood at high $x$, we will extract the higher twist piece of the spin structure function $\bar{g}_2$ and evaluate the quantity $d_2^n = \int_0^1 \bar{g}_2\, dx = \int_0^1 x^2(2g_1 + 3g_2)\, dx$ at *constant* $Q^2$ for the very first time for $Q^2 > 1\ \mathrm{GeV}^2/c^2$. All previous measurements of $d_2^n$ at higher $Q^2$ have required data taken over a broad range of $Q^2$ values to be evolved to some common $Q^2$ prior to evaluating the $d_2$ integral. At higher $x$, this evolution has required the transform from $Q^2$'s of as much as $15\,\mathrm{GeV}^2/c^2$ down to $5\,\mathrm{GeV}^2/c^2$.

$d_2$ is related to the twist three matrix element in the Operator Product Expansion (OPE) framework and is connected to the quark-gluon correlations within the nucleon. The quantity $d_2^n$ reflects the response of the *color* electric and magnetic fields to the polarization of the nucleon (alignment of its spin along one direction). This quantity has seen thorough study in Lattice QCD and is one of the cleanest observables with which to test the theory.

We plan to extract the spin structure functions $g_1^n$ and $g_2^n$ by measuring parallel and perpendicular asymmetries using the SHMS and upgraded HMS in Hall C. We will use the longitudinally polarized ($P_b$ = 0.80) CEBAF electron beam at 11 GeV and a 40 cm-long high pressure polarized $^3$He target. Both the SHMS and the HMS will be operated in "single-arm" mode (*vs.* coincidence mode) to measure two different kinematic bites for each of three 200 hour floor configurations. The target polarization orientation will be set transverse or longitudinal to the beam with a value of $P_t$ = 0.50 while the beam helicity will be reversed at a rate of 30 Hz. A beam current of 10 $\mu$A combined with a 40 cm long target of density 12 amg provides a luminosity of $6.7 \cdot 10^{35}$ cm$^{-2}$s$^{-1}$. With the inclusion of an additional 100 hours for overhead and calibration, the total beam request is 700 hours, or roughly 29 days of beam.

The upgraded SHMS/HMS combination in Hall C at Jefferson Lab provides an ideal facility for this measurement. The large momentum acceptance of the SHMS allows a very broad $x$ region to be measured over nearly constant $Q^2$ in a single kinematic setting. The HMS can then be used to simultaneously fill in gaps in the low-$x$ region, resulting in nearly contiguous $x$ coverage over a broad $Q^2$ band – something that has never before been accomplished. The combined data will allow the extraction of $d_2^n(Q^2)$ at truly constant $Q^2$'s of 3, 4, and $5\,\mathrm{GeV}^2/c^2$. The precision with which these values may be measured, combined with explicit information on the $Q^2$ evolution of $d_2$ provide a strict test of Lattice QCD.

We would also like to comment on a "sister" experiment in Hall A that has also been submitted to the PAC30 board. The kinematic coverage of the Hall A measurement has been specifically selected to compliment the coverage of the Hall C proposal. BigBite in Hall A is ideally suited to map out the the high-$x$, high-$Q^2$ region is reasonable time and without tying up the highest energy Hall. In contrast, the SHMS/HMS in Hall C is uniquely suited to make a definitive measurement of the $Q^2$ evolution of $d_2^n$ due to its remarkably flat $Q^2$ coverage per bin over $0.4 < x < 1$. BigBite is not able to match this feat due to rate limitations were it moved sufficiently far forward. Together, the two measurements would provide a truly exceptional understanding of the structure function $g_2^n(x,Q^2)$, $d_2^n(Q^2)$, and the associated quark-gluon correlations within the nucleon.

# Contents

# 1 Technical participation of research groups

After thorough discussion with Hall C and JLab administration, Temple University, the College of William and Mary, and the University of Kentucky will jointly commit to providing two full-time equivalent (FTE) manpower to the upgrade of Hall A. The Chinese collaboration (USTC and CIAE) intend to commit an additional 1–2 FTE manpower. This effort will be devoted to successfully commissioning the following base equipment items:

- Compton polarimeter,
- Moeller polarimeter,
- ARC beam energy measurement, and the
- Double fast-raster system.

These personnel would be assigned to work in conjunction with the dedicated Hall C staff. Funding for these FTE's will come from existing DOE grants and the institutions involved and will *not* constitute an additional DOE funding request.

Beyond the baseline equipment, the polarized $^3$He group will facilitate the development and installation of the polarized 3He target for Hall C. This target has seen tremendous demand at JLab in recent years and will no doubt be an equally critical component for Hall C's 12 GeV program.

## 2 Introduction and Motivation

In inclusive polarized lepton-nucleon deep-inelastic scattering, one can access two spin-dependent structure functions of the nucleon, $g_1$ and $g_2$. In the last twenty five years, measurements of $g_1$ have been used to test Quantum Chromodynamics (QCD) through the Björken sum rule and investigate the spin content of the nucleon in term of its constituents. While $g_1$ can be understood in terms of the Feynman parton model which describes the scattering in terms of *incoherent* parton scattering, $g_2$ cannot. Rather, one has to consider parton correlations initially present in the target nucleon, and the associated process is given a *coherent* parton scattering in the sense that more than one parton takes part in the interaction. Indeed, using the operator product expansion (OPE) [6, 7], it is possible to interpret the $g_2$ spin structure function beyond the simple quark-parton model as a higher twist structure function. As such, it is exceedingly interesting because it provides a unique opportunity to study the quark-gluon correlations in the nucleon which cannot otherwise be accessed.

In a recent review Filippone and Ji [8] explained that most higher-twist processes cannot be cleanly separated from the leading twist because of the so-called infrared renormalon problem first recognized by t'Hooft. This ambiguity arises from separating quarks and gluons pre-existing in the hadron wave function from those produced in radiative processes. Such a separation turns out to be always scheme dependent. However, the $g_2$ structure function is an *exception* because it contributes at the leading order to the spin asymmetry of longitudinally-polarized lepton scattering on transversely-polarized nucleons. Thus, $g_2$ **is among the cleanest higher-twist observables**.

Why does the $g_2$ structure function contain information about the quark and gluon correlations in the nucleon? From the optical theorem, $g_2$ is the imaginary part of the spin-dependent Compton amplitude for the process $\gamma^*(+1)+N(+1/2) \rightarrow \gamma^*(0)+N(-1/2)$,

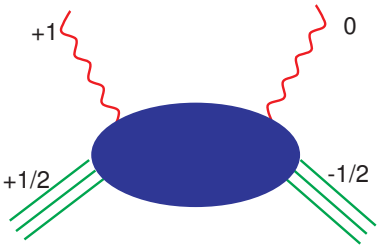


Figure 1: Compton amplitude of $\gamma^*(+1)+N(+1/2) \rightarrow \gamma^*(0)+N(-1/2)$.

where $\gamma^*$ and $N$ denote the virtual photon and the nucleon, respectively, and the numbers in the brackets are the helicities. Thus this Compton scattering involves the $t$-channel helicity exchange $+1$. When factorized in terms of parton sub-processes, the intermediate partons must carry this helicity exchange. Because chirality is conserved in vector coupling, massless quarks in perturbative processes cannot produce a helicity flip. QCD allows this helicity exchange to occur in two ways (see Fig. 2): first, single quark scattering in which the quark carries one unit of orbital angular momentum through its transverse momentum wave function; second, quark scattering with an additional transversely-polarized gluon from the nucleon target. The two mechanisms are combined in such a way to yield a gauge-invariant result. Consequently, $g_2$ provides a direct probe of the quark-gluon correlations in the nucleon wave function.

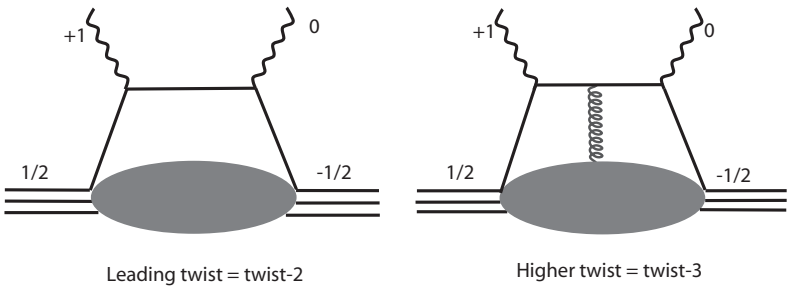


Figure 2: Twist-two and twist-three contributions to virtual Compton scattering

### 2.1 The twist-three reduced matrix element

The piece of interesting physics we want to focus on in this proposal is contained in the second moment in $x$ of a linear combination of $g_1$ and $g_2$, namely

$$\begin{aligned} d_2(Q^2) &= \int_0^1 x^2 \left[2g_1(x,Q^2) + 3g_2(x,Q^2)\right] dx \quad (1) \\ &= 3\int_0^1 x^2 \left[g_2(x,Q^2) - g_2^{WW}(x,Q^2)\right] dx \quad (2) \\ &= 3\int_0^1 x^2 \left[\bar{g_2}(x,Q^2)\right] dx \end{aligned}$$

where $g_2^{WW}$, known as the Wandzura-Wilczek [9] term, depends only on $g_1$

$$g_2^{WW}(x,Q^2) = -g_1(x,Q^2) + \int_x^1 \frac{g_1(y,Q^2)}{y} dy. \quad (3)$$

and

$$\bar{g_2}(x,Q^2) = -\int_x^1 \frac{dy}{y}\frac{d}{dy}\left[\frac{m}{M}h_T(y,Q^2) + \xi(y,Q^2)\right] \quad (4)$$

is expressed in terms of the transverse polarization density $h_T(x,Q^2)$ function (Transversity) suppressed by the quark mass $m$ over the nucleon mass $M$ and the twist-3 term $\xi$ which arises from quark-gluon correlations.

It is interesting to note that the quantity $d_2$ also appears in the first moment of $g_1$ when at large $Q^2$ ($Q^2 \gg \Lambda^2_{QCD}$) it is expressed in terms of a twist expansion [13, 12]:

$$\Gamma_1(Q^2) = \int_0^1 g_1(Q^2,x)dx = \frac{1}{2}a_0 + \frac{M^2}{9Q^2}\left(a_2 + 4d_2 + 4f_2\right) + O\left(\frac{M^4}{Q^4}\right), \quad (5)$$

where $a_0$ is the leading twist, dominant contribution. It is determined, apart from QCD radiative corrections [14], by the triplet $g_A$ and octet $a_8$ axial charges and the net quark spin contribution to the total nucleon spin. These axial charges are extracted from measurements of the neutron and hyperons weak decay measurements [15]. Here $a_2$ is a second moment of the $g_1$ structure function and arises from the target mass correction [12]. The quantities $d_2$ and $f_2$ are the twist-3 and the twist-4 reduced matrix elements. These matrix elements contain non-trivial quark-gluon interactions beyond the parton model. A first extraction of $f_2$ has been carried by Ji and Melnitchouk in [16] using the world data but with poor statistical precision below $Q^2$ = 1 GeV$^2$. Other investigations of higher twist contributions in the case of spin-dependent structure

functions were performed and reported in Ref. [17, 18]. Recent extractions of $f_2$ separately for the neutron and the proton as well as the non-singlet combination $f_2^{p-n} = f_2^p - f_2^n$ have also been carried out combining the existing high $Q^2$ world data with new low $Q^2$ data from Jefferson Lab [19, 20, 21, 22]. The new data helped gauge the size of higher twist contribution (beyond twist-4), thus checking the convergence of the expansion, and providing for an improved precision in the extraction of $f_2$.

In QCD, $d_2$ and $f_2$ can be expressed as linear combinations of the induced color electric and magnetic polarizabilities $\chi_E$ and $\chi_B$ [8, 23] when a nucleon is polarized. This twist expansion may be valid down to $Q^2 \approx 1$ GeV$^2$ if higher order terms are small.

At large $Q^2$ where an OPE expansion becomes valid, the quantity $d_2$ reduces to a twist-3 matrix element which is related to a certain quark-gluon correlation.

$$d_2 S^{[\mu} P^{\{\nu]} P^{\lambda\}} = \frac{1}{8} \sum_q \langle P,S|\bar{\psi}_q \, g\widetilde{F}^{\{\mu\nu}\gamma^{\lambda\}}\psi_q|P,S\rangle \ , \tag{6}$$

where $g$ is the QCD coupling constant, $\widetilde{F}^{\mu\nu} = (1/2)\varepsilon^{\mu\nu\alpha\beta}F_{\alpha\beta}$, $F_{\alpha\beta}$ are the gluon field operators, and the parentheses $\{\cdots\}$ and $[\cdots]$ denote symmetrization and antisymmetrization of indices, respectively. The structure of the above operator suggests that it measures a quark *and* a gluon amplitude in the initial nucleon wavefunction [6, 7].

The twist-4 contribution is defined by the matrix element

$$f_2 \, M^2 S^\mu \ = \ \frac{1}{2} \sum_q e_q^2 \, \langle P,S|g \, \bar{\psi}_q \, \widetilde{F}^{\mu\nu}\gamma_\nu \, \psi_q|P,S\rangle \ , \tag{7}$$

where $\widetilde{F}^{\mu\nu}$ is the dual gluon field strength tensor. $f_2$ can also be defined (generalized) in terms of the structure functions:

$$f_2(Q^2) = \frac{1}{2}\int_0^1 dx \, x^2 \Big( 7g_1(x,Q^2) + 12g_2(x,Q^2) - 9g_3(x,Q^2) \Big), \tag{8}$$

where $g_3$ is the 3rd spin structure function, which has not yet been measured but could be accessed by an asymmetry measurement of unpolarized lepton scattering off a longitudinally polarized target. With only $g_1$ and $g_2$ data available, $f_2$ can also be extracted through Eqn. 5 if the twist-6 or higher terms are not significant.

The physical significance of $d_2(Q^2)$ has been articulated by Ji and we quote,

> *[W]e ask when a nucleon is polarized in its rest frame, how does the gluon field inside of the nucleon respond? Intuitively, because of the parity conservation, the color magnetic field $\vec{B}$ can be induced along the nucleon polarization and the color electric field $\vec{E}$ in the plane perpendicular to the polarization.*

After introducing the color-singlet operators $O_B = \psi^\dagger g\vec{B}\psi$ and $O_E = \psi^\dagger \vec{\alpha} \times g\vec{E}\psi$, we can define the gluon-field polarizabilities $\chi_B$ and $\chi_E$ in the rest frame of the nucleon[10, 11]

$$\langle PS|O_{B,E}|PS\rangle = \chi_{B,E} 2M^2 \vec{S} \, . \tag{9}$$

Then $d_2$ can be written as

$$d_2 = (\chi_E + 2\chi_B))/8 \, . \tag{10}$$

Thus $d_2$ is a measure of the response of the color electric and magnetic fields to the polarization of the nucleon. The reduced matrix element $f_2$ can be expressed also as a different linear combination of the same color polarizabilities

$$f_2 = (\chi_E - \chi_B)/3 \, . \tag{11}$$

Ultimately the color electric and magnetic polarizabilities will be obtained from $d_2(Q^2)$ and $f_2(Q^2)$ when high precision data on both $g_1$ and $g_2$ become available. In this proposal we are aiming at mapping out the $(x,Q^2)$ behavior of $g_2$ and providing significantly enhanced data for $d_2^n$ at large $Q^2$.

## 2.2 Burkhardt-Cottingham Sum rule

The $g_2$ structure function itself obeys the Burkhardt-Cottingham (BC) sum rule [25]

$$\Gamma_2(Q^2) = \int_0^1 g_2(x,Q^2)\, dx = 0\ , \tag{12}$$

which was derived from the dispersion relation and the asymptotic behavior of the corresponding spin-flip Compton amplitude. This sum rule is true at all $Q^2$ and does not follow from the OPE. It is rather a super-convergence relation based on Regge asymptotics as articulated in the review paper by Jaffe [26]. Many scenarios which could invalidate this sum rule have been discussed in the literature [7, 27, 28]. However, this sum rule was confirmed in perturbative QCD at order $\alpha_s$ with a $g_2(x,Q^2)$ structure function for a quark target [29]. Surprisingly a first precision measurement of $g_2$ by the E155 collaboration [24] at $Q^2$ = 5 GeV$^2$ but within the experimentally limited range of $x$ has revealed a violation of this sum rule on the proton at the level of three standard deviations. In contrast, the neutron sum rule is poorly measured but consistent with zero within one standard deviation. New high precision neutron $g_2$ data [30, 31] shown in Fig. 6 at $Q^2$ below 1 GeV suggest that the BC sum rule is verified within errors. While a full test of the BC sum rule cannot be performed within the limited $x$ range of this proposal, this measurement will provide useful data to further explore the large $x$ contributions to the sum rule in the neutron/$^3$He.

## 3 Experimental status of $d_2^{p,n}(Q^2)$ and $\Gamma_2^n(Q^2)$ measurements

The early measurements of the $g_2$ spin structure function performed by the SMC [32] and E142 [33, 34] collaborations in the 90's were meant to reduce the systematic errors when extracting $g_1$ due to $g_2$'s contribution to the measured parallel asymmetries. As the statistical precision of $g_1$ improved, a better measurement of $g_2$ was required to minimize the error on $g_1$. Therefore, in SLAC E143 [35], E154 [36] and E155 [37] more data on $g_2$ were collected and $d_2$ was evaluated and published by these collaborations. But since the statistical errors of these experiments were still large and as the interest in the physics of $g_2$ rose, a dedicated experiment known as SLAC E155x [38] was approved to measure $g_2$ at relatively large $Q^2$ to investigate the higher twist effects in the proton and deuteron. This led to an evaluation of $d_2$ with much improved statistical precision compared to what existed previously for both the proton and the deuteron [38]. At lower $Q^2$ another dedicated experiment known as JLab E97-103 [40] was performed at Jefferson Lab to look for higher twists effects by exploring the $Q^2$ evolution of $g_2^n$ using a polarized $^3$He target from $Q^2$ = 1.4 GeV$^2$ down to $Q^2$ = 0.6 GeV$^2$ at $x$ = 0.2. The statistical precision was improved by almost an order of magnitude. Two other JLab experiments, E99-117 [39] and E94-010 [30, 31], had the opportunity to measure the $g_2$ structure function in a non-dedicated mode while focusing on a measurement of the $g_1^n$ structure function. The first one provided three data points in the valence quark DIS region $(x, Q^2)$ = (0.33, 2.71), (0.47, 3.52) and (0.6, 4.83) while the second one was carried out in the resonance region at $Q^2$ below 1 GeV$^2$.

Fig. 3 shows $d_2$ from SLAC E155X for the proton in the upper panel and the SLAC E155x and JLab E99-117 combined neutron result compared to several calculations. The proton result is generally consistent with the chiral quark model [61, 46] and some bag models [47, 12, 16] while one to two standard deviations away from the QCD sum rule calculations [48, 49, 50]. More importantly, the comparison with the recent lattice QCD calculation of the QCDSF collaboration [51] shows consistency with the experimental datum of the proton. However, it clearly indicates the need for an improvement on the experimental precision for the neutron datum. In fact Jefferson Lab E99-117 measurements of $g_2^n$ at large $x$ combined with SLAC E155X have improved on the total error by almost a factor of two. At the same time the latest QCDSF lattice calculation reported here has improved also by a factor of two compared to their previous results published in 2001 [52]. Of course it is difficult to guess the total error on the lattice calculation but at this time the neutron $d_2$ result is two standard deviations away from the experimental value including the lattice and chiral extrapolation errors. The experimental error bar is still dominated by the statistical uncertainty.

The Lattice Hadron Physics Collaboration (LHPC) based at Jefferson Lab has plans to extract this matrix element for the proton and the neutron [53] and provides a different check on the QCDSF collaboration lattice calculations.

It is worth noting that, except for the QCD sum rule calculation, all nucleon bag models or chiral soliton models predict values consistent with the lattice QCD result. The experimental result is thus $2\sigma$ away from zero all available calculations. In these models $g_2^n$ is negative at large $x$, therefore it is conceivable that the poor precision (Fig. 5) of the data in this region is affecting the overall sign of the result. It is important to note that from the point of view of a simple quark model, the $d_2$ matrix element of the neutron should be much smaller than that of the proton because of SU(6) spin-flavor symmetry. Thus, with the present precision of the combined SLAC E155x and JLab E99-117 neutron data it is difficult to draw any conclusions on the sign and size of the neutron higher twist (twist-three) contribution. However because $d_2$ is a second moment in $x$ of the linear combination $(2g_1 + 3g_2)$ the neutron data set can be improved significantly at Jefferson Lab with a dedicated measurement like the one proposed here. Due to the $x^2$ weighting, the contribution of the small $x$ region is suppressed and thus using the existing world data to cover the region $x < 0.23$ should be sufficient to complete the integral.

During JLab experiment E94-010 [30], which was aimed at measuring the Gerasimov-Drell-Hearn extended sum, data on $g_2$ were taken using a polarized $^3$He target across the resonance in the range $0.1 < Q^2 < 0.9$ GeV$^2$. New results on two moments of the neutron spin structure functions, $\Gamma_2^n$ and $d_2^n$, are now avail-

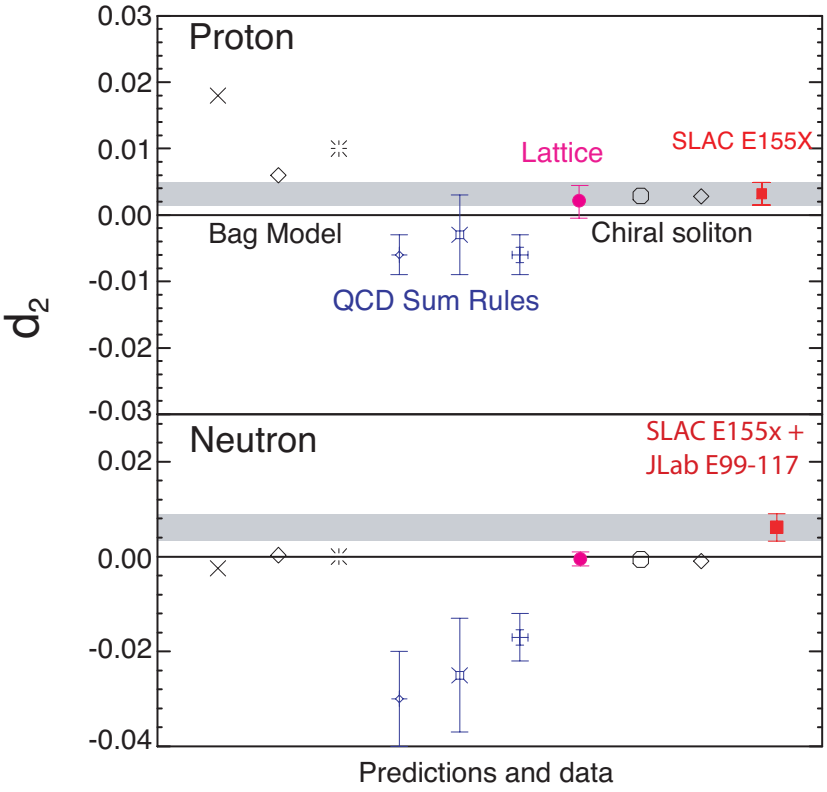


Figure 3: $d_2$ SLAC E155X results of the proton and SLAC E155x combined with JLab E99-117 results of the neutron results compared to several theoretical calculations including lattice QCD (see text). Upper panel is for the proton and lower panel is for the neutron.

able from this experiment. These low $Q^2$ results are shown in Fig. 4 along with the SLAC E155x and JLab E99-117 combined results. The results published in [31] give a glimpse of the $Q^2$ evolution of the quantity $\bar{d}_2^n$ which does not include the elastic contribution (at $x = 1$) to the integral. However this contribution is negligible above $Q^2$= 3 GeV$^2$ but dominate the quantity $d_2$ below $Q^2$ = 1 GeV$^2$. Note that no comparable data exist for the proton.

In the investigation of higher twists contributions an important step has already been taken with JLab experiment E97-103 [40], which has provided precision data of $g_2^n$ in the deep inelastic region and determined its $Q^2$ evolution in the range $0.56 < Q^2 < 1.4$ GeV$^2$ for a fixed value of $x \approx 0.2$. The unprecedented statistical accuracy achieved in JLab E97-103 was critical to probe the size of higher twists contributions by comparing directly the measured $g_2^n$ to the leading twist contribution ( the twist-two contribution known as $g_2^{n(WW)}$ [42]). The experiment has been completed and the results published [40] showing a small but finite size of higher twists as $Q^2$ decreases below 1 GeV$^2$. However, as the coverage was in the low-$x$ region, this experiment has little impact on the evaluation of the $d_2$ integral. Note that this does not diminish its importance for direct comparison between the measured $g_2$ and the leading twist piece of $g_2$.

Two other recently completed experiments, JLab experiment E01-012 [43] which used a polarized $^3$He target, and JLab experiment E01-006 [44] which uses polarized $NH_3$ and $ND_3$ targets, will add to the wealth of neutron spin structure functions data ($g_1^n$ and $g_2^n$) in the resonance region. However, the first measurement emphasizes the investigation of $g_1$ while the second provides data at $Q^2$ = 1.3 GeV$^2$ for $g_2^p$

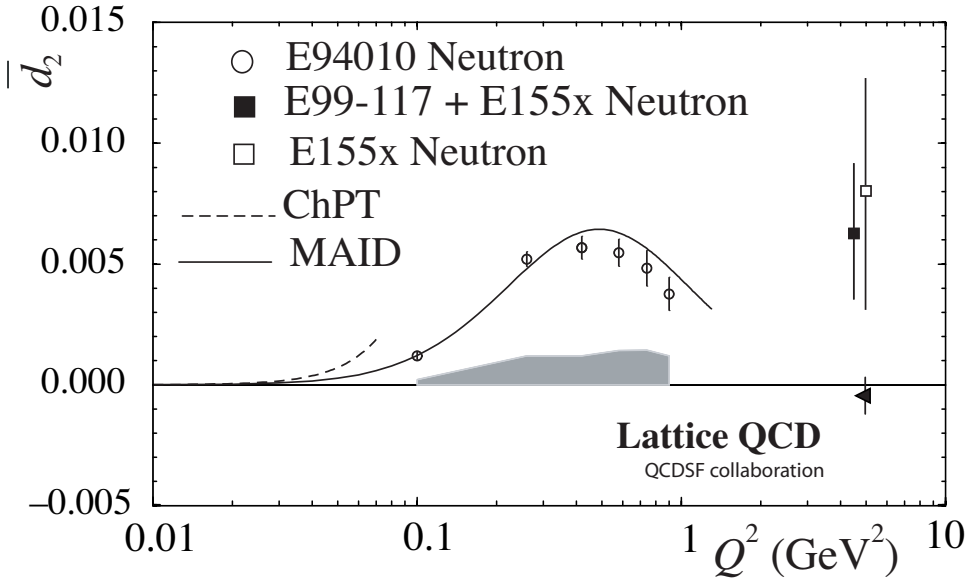


Figure 4: $\bar{d_2}(Q^2)$ results of JLab E94-010 without the nucleon elastic contribution are presented. The grey band represents their corresponding systematic uncertainty. The SLAC E155 [38] neutron result is also shown here (open square). The solid line is the MAID calculation[55] while the dashed line is a HB$\chi$PT calculation[56] valid only at very low $Q^2$. The lattice prediction [51] at $Q^2$ = 5 GeV$^2$ for the neutron $d_2$ reduced matrix element is negative but consistent with zero. We note that all models shown in Fig. 3 predict a negative value or zero at large $Q^2$ where the elastic contribution is negligible. At moderate $Q^2$ the data show a positive $\bar{d_2^n}$, and indicate a slow decrease with $Q^2$. The combined SLAC+JLab datum shows a positive $d_2^n$ value but with still a large error bar.

with high precision but limited precision for $g_2^n$.

We summarize the situation of the quality of the neutron $g_2$ spin structure data in Fig. 5 where we report the world data with $Q^2$ greater than 1 GeV$^2$, the projected results of the approved JLab experiment E06-014, and show a comparison with some model calculations as well as the Wandzura-Wilczek $g_2^{WW}$ contribution to $g_2$. The neutron $g_2$ extracted from the proton and deuteron measurements of E155X are also shown. The statistical accuracy already achieved in JLab E97-103 is displayed for their highest $Q^2$ kinematics point at $Q^2 = 1.4\,\mathrm{GeV}^2$, $x = 0.2$.

We should point out that in this proposed experiment, unlike in previous experiments, world data fits of $R = \sigma_L/\sigma_T$, $F_2$ and $g_1$ will *not* be used to evaluate $g_2$. Rather, we shall measure absolute polarized cross sections for both directions of the target spin, parallel and perpendicular and extract $g_2$. Furthermore, in order to evaluate $d_2$ in those experiments, it was common practice to evolve the measured $g_2$ data from the measured $Q^2$ to a common $Q^2$ value, however, this evolution is not well understood for the twist-three part of $g_2$, namely $\bar{g_2}$. In contrast, our data will be measured at a constant Q$^2$ and for three separate values of $Q^2$.

The proposed measurement is optimized to minimize the error on the determination of $g_2^n$. Obviously, the ultimate statistical precision at each $x$ value will help for stringent comparison with models of $g_2^n(x, Q^2)$.

Finally, turning to the BC sum rule, the experimental situation is summarized in Fig. 6 where we show $\Gamma_2^n$ measured in E94-010 (solid circles) and, including the elastic contribution (open circles) evaluated using a dipole form factor for $G_M^n$ and the Galster fit for $G_E^n$. The positive light grey band corresponds to the total experimental systematic errors while the dark negative band represents an estimated DIS contribution

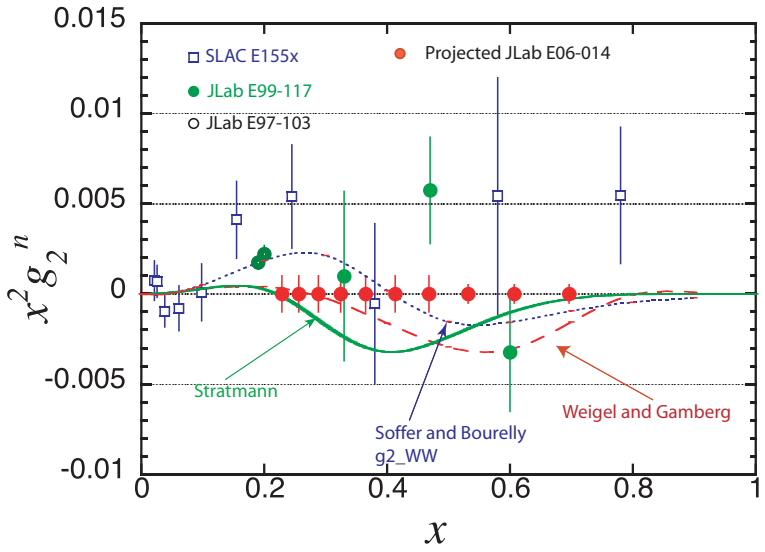


Figure 5: Present world $x^2 g_2^n$ data for $Q^2 \geq 1$ GeV$^2$ along with some model calculations and $g_2^{WW}$. SLAC E155X neutron results are derived from measurements using polarized $NH_3$ and $ND_3$ targets as described in Ref.[41, 24]. The JLab experiments used a polarized $^3$He target in Hall A. We note the consistency between the data. The solid curve is a quark model calculation by Stratmann [47], the dashed line is a chiral soliton calculation by Weigel and Gamberg [61]. The dotted line represent the evaluation of $g_2^{WW}$ using $g_1$ from the statistical model of the nucleon by Bourelly and Soffer [54].

using $g_2^{WW}$. The solid line is the resonance contributions evaluated using MAID and the negative light-grey band is the neutron elastic contribution added to the measured data to determine $\Gamma_2^n$. The results are quite encouraging since the data show that the BC sum rule is verified within uncertainties over the $Q^2$ range measured. Our result is at odds with the reported violation of this sum rule on the proton at high $Q^2$ (where the elastic contribution is negligible) [24]. It is, however, consistent with the neutron result of SLAC E155 (open square) which unfortunately has a rather large error bar. In light of our results, a high statistical precision measurement in the range 1 GeV$^2 \leq Q^2 \leq 5$ GeV$^2$ would be very useful for both the proton and neutron even if the $x$ range is limited.

In the next section we shall describe how we plan to improve on the statistical precision of the $g_2$ neutron data at large $x$ which will result in a reduction of the statistical error bar of $d_2^n$ by a factor of almost four as well as provide a reasonable add-on to the BC sum evaluations at $< Q^2 >$ = 3, 4 and 5 GeV$^2$.

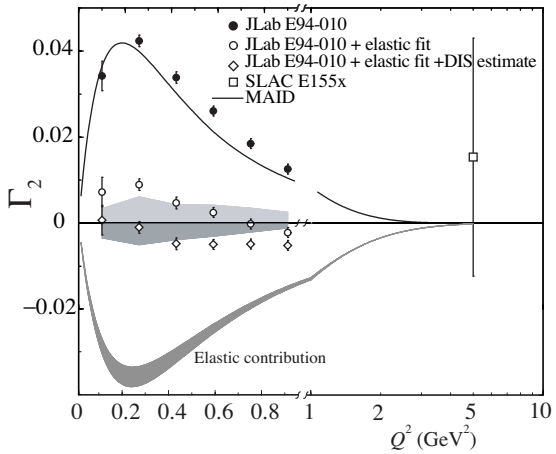


Figure 6: Results of $\Gamma_2^n$ (open diamonds) along with the average of the world data from DIS. The theoretical prediction for this quantity is zero (see text).

# 4 The Proposed Experiment

## 4.1 Choice of Kinematics (SHMS/HMS)

The unique feature of the SHMS spectrometer is its combination of large momentum and large target length acceptance. In addition, the SHMS will be capable of accepting event rates up to 10 kHz and will have a $e^-$:$h$ discrimination of at least 1000:1. Such specifications are ideal to efficiently measure the $Q^2$ dependence of spin structure functions, here $g_2^n$, over a large range of $x$. Proper choice of kinematic settings will allow us to measure $d_2^n$ at nearly constant values of $Q^2$.

We plan to extract $g_1^n$ and $g_2^n$ by measuring parallel and perpendicular asymmetries. The directions are defined relative to the momentum of the incoming electron beam. The asymmetries can be written as

$$A_{\parallel} = \frac{1}{F_1(x,Q^2)}\frac{1-\varepsilon}{\nu(1+\varepsilon R(x,Q^2)}(g_1^n(E+E'cos(\theta)) - \frac{Q^2}{\nu}g_2^n), \quad (13)$$

$$A_{\perp} = \frac{1}{F_1(x,Q^2)}\frac{1-\varepsilon}{\nu(1+\varepsilon R(x,Q^2)}E'sin(\theta)(g_1^n + \frac{2E}{\nu}g_2^n). \quad (14)$$

Using Eqns. 13 and 14 for the extraction of $g_1^n$ and $g_2^n$ relies on the knowledge of the unpolarized structure function $F_1^n(x,Q^2)$. This structure function is related to $F_2^n(x,Q^2)$ (via the Callan-Gross relation) and has been measured over a large kinematic range. A variety of existing parton distribution functions can be used to reproduce the $F_2^n$ structure function well. At large values of $Q^2$ and $x$ the nucleon resonances disappear and global (and local) Bloom-Gilman duality is well established. A different and more direct way to access the spin structure functions is the measurement spin dependent cross sections. The cross section differences for longitudinally and transversely polarized targets are given by

$$\frac{d^2\sigma^{\downarrow\Uparrow}}{d\Omega dE'} - \frac{d^2\sigma^{\uparrow\Uparrow}}{d\Omega dE'} = \frac{4\alpha^2 E'}{Q^2 EM\nu}\left[(E+E'cos(\theta))g_1(x,Q^2) - 2xMg_2(x,Q^2)\right], \quad (15)$$

$$\frac{d^2\sigma^{\downarrow\Leftarrow}}{d\Omega dE'} - \frac{d^2\sigma^{\uparrow\Leftarrow}}{d\Omega dE'} = \frac{4\alpha^2 E'}{Q^2 EM\nu}E'sin(\theta)\left[g_1(x,Q^2) - \frac{4xEM}{Q^2}g_2(x,Q^2)\right]. \quad (16)$$

Using the last two equations for the extraction of $g_1$ and $g_2$ does not require the knowledge of $F_1^n$. We plan to use the spectrometers to measure the spin dependent cross sections directly.

The rates and statistical uncertainties were estimated using the parameters listed in Table 1. The parametrization MRST2001LO [1] for parton distribution functions was used to construct the unpolarized structure functions. The range of validity of this parametrization is estimated to be $1.0\times10^{-5} \le x \le 1.0$ and $1.25 \le Q^2 \le 1.0\times10^7$ GeV$^2$. Two additional parametrizations (CTEQ61 [2] and H12000LO [3]) were used to study the variations in the counting rates at one representative kinematic setting. The agreement was better than 10%. Figure 7 plots the kinematic coverage in $(x,Q^2)$ of this proposal.

Table 2 summarizes the proposed binning and expected rates for the three SHMS kinematics. Note that this corresponds to a single SHMS spectrometer setting. The total momentum bite at each $\theta_0$ was split into four equally spaced momentum bins. Table 3 shows the expected rates for the three HMS kinematic settings.

The parallel vs. perpendicular running times were estimated in two independent ways: i) minimization of the statistical uncertainty in $g_2^n$ and ii) minimization of the statistical uncertainty in $x^2(2g_1+3g_2)$. Both methods yielded essentially the same time distribution.

The electron rates quoted in Tables 2 and 3 are the rates from $^3$He only. Additional rates from small admixtures of the buffer gas nitrogen were checked and can be neglected. Scattering from the end windows will be minimized using software cuts.

Table 1: Parameters used for the SHMS rate estimates

| | SHMS | | | HMS | | |
|---|---|---|---|---|---|---|
| kinematic setting | I | II | III | I | II | III |
| beam energy | 11 GeV | | | | | |
| beam current | 10 $\mu$A | | | | | |
| beam polarization | 0.8 | | | | | |
| scattering angle | 11.0° | 13.3° | 15.5° | 13.5° | 16.4° | 20.0° |
| momentum range | -15% → +25% | | | -10% → +10% | | |
| z-acceptance (at 90°) | 50 cm | | | 10 cm | | |
| solid angle | 4 msr | | | 8.1 msr | | |
| efficiency | 0.80 | | | | | |
| target length | 40 cm | | | | | |
| target polarization | 0.50 | | | | | |
| eff. target density | 10.3 amg | | | | | |

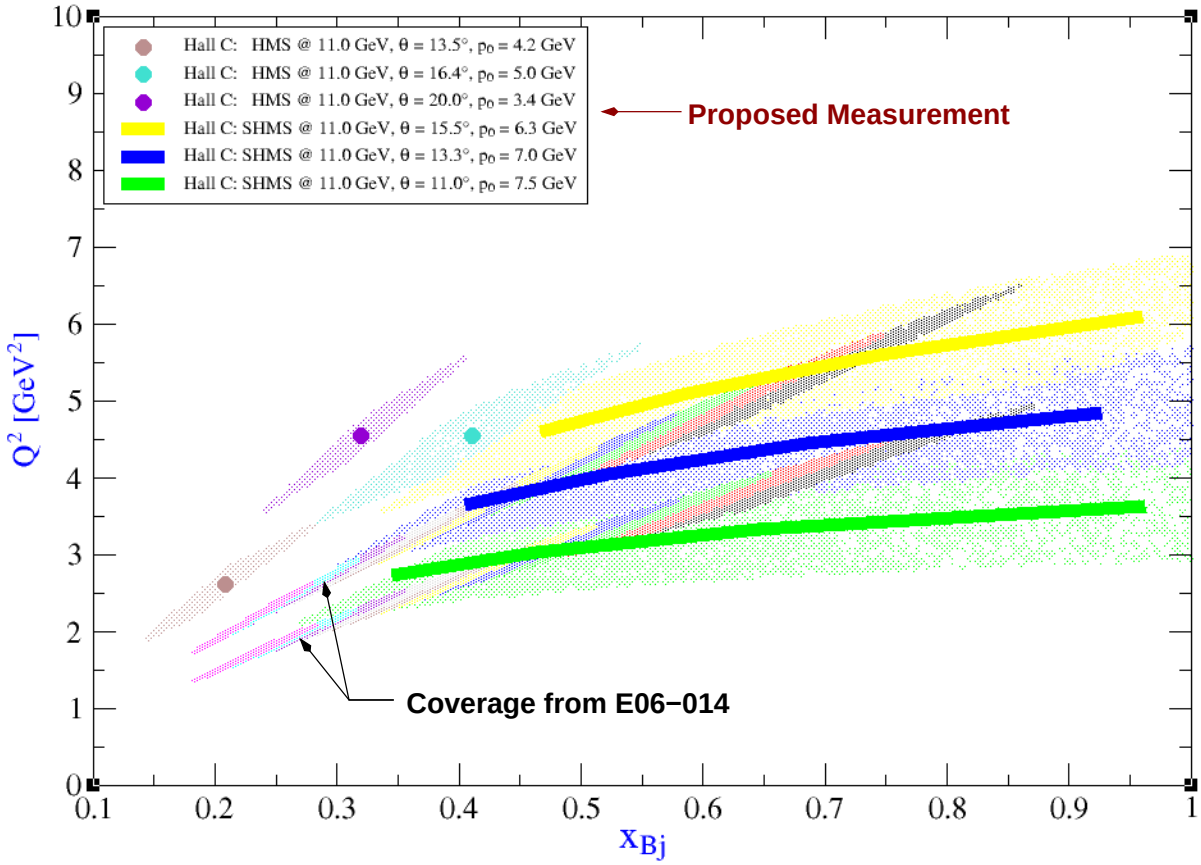


Figure 7: Kinematic coverage for the six kinematic settings for the proposed experiment. The three SHMS bands will be subdivided into four bins each during offline analysis. The multicolored stripes reflect the coverage from the lower energy measurement E06-014.

Table 2: Kinematic bins and expected rates for the SHMS. The uncertainties for $A_{\parallel}$ and $A_{\perp}$ are *statistical* only.

| SHMS Setting | $E'_{bin}$ [GeV] | $Q^2$ [GeV$^2$] | x | W [GeV] | $e^-$ rate [Hz] | $\pi^-$ rate [Hz] | $t_{\parallel}$ [hrs] | $t_{\perp}$ [hrs] | $\Delta A_{\parallel}$ [$\cdot 10^{-4}$] | $\Delta A_{\perp}$ [$\cdot 10^{-4}$] |
|---|---|---|---|---|---|---|---|---|---|---|
| $\theta_0 = 11^\circ$ | 6.772 | 2.737 | 0.345 | 2.468 | 213.3 | 4.9 | 15 | 185 | 3.1 | 0.85 |
| | 7.511 | 3.036 | 0.463 | 2.098 | 161.3 | 1.0 | 15 | 185 | 3.5 | 0.98 |
| $E'_{cent} = 7.5$ | 8.251 | 3.335 | 0.646 | 1.648 | 64.8 | 0.21 | 15 | 185 | 5.4 | 0.16 |
| GeV | 8.990 | 3.634 | 0.963 | 1.013 | 0.17 | 0.037 | 15 | 185 | 100 | 30 |
| $\theta_0 = 13.3^\circ$ | 6.193 | 3.654 | 0.405 | 2.502 | 66.5 | 2.1 | 17 | 183 | 5.3 | 1.5 |
| | 6.867 | 4.052 | 0.522 | 2.144 | 42.8 | 0.38 | 17 | 183 | 6.4 | 1.9 |
| $E'_{cent} = 7.0$ | 7.541 | 4.450 | 0.685 | 1.713 | 14.8 | 0.063 | 17 | 183 | 11 | 3.3 |
| GeV | 8.215 | 4.847 | 0.927 | 1.127 | 0.12 | 0.0094 | 17 | 183 | 120 | 37 |
| $\theta_0 = 15.5^\circ$ | 5.749 | 4.600 | 0.466 | 2.480 | 24.0 | 0.83 | 20 | 180 | 8.4 | 2.6 |
| | 6.372 | 5.098 | 0.587 | 2.117 | 12.8 | 0.15 | 20 | 180 | 11 | 3.5 |
| $E'_{cent} = 6.3$ | 6.996 | 5.597 | 0.744 | 1.676 | 3.3 | 0.025 | 20 | 180 | 22 | 7.0 |
| GeV | 7.619 | 6.096 | 0.960 | 1.067 | 0.015 | 0.0037 | 20 | 180 | 320 | 110 |

Table 3: Expected rates for the three HMS settings. The uncertainties for $A_{\parallel}$ and $A_{\perp}$ are *statistical* only.

| $\theta_0$ [$\circ$] | $E'_{cent}$ [GeV] | $Q^2$ [GeV$^2$] | x | W [GeV] | $e^-$ rate [Hz] | $\pi^-$ rate [Hz] | $t_{\parallel}$ [hrs] | $t_{\perp}$ [hrs] | $\Delta A_{\parallel}$ [$\cdot 10^{-4}$] | $\Delta A_{\perp}$ [$\cdot 10^{-4}$] |
|---|---|---|---|---|---|---|---|---|---|---|
| 13.5 | 4.305 | 2.617 | 0.208 | 3.293 | 221.3 | 282.0 | 12 | 188 | 3.2 | .83 |
| 16.4 | 5.088 | 4.555 | 0.410 | 2.727 | 64.9 | 6.4 | 17 | 183 | 5.2 | 1.6 |
| 20.0 | 3.529 | 4.682 | 0.334 | 3.200 | 21.3 | 28.6 | 15 | 185 | 9.3 | 2.7 |

Another source of background are electrons from $e^+/e^-$ pair creation. We assumed the positrons are generated from Dalitz decays of $\pi^0$'s and conversion of decay photons in the target and materials surrounding the target. The positrons are then detected in the spectrometer. A reasonable approximation for this background estimate is taking the average of $\pi^-$ and $\pi^+$ rates [4]. The cross sections were obtained from fits by D. Wiser [5]. Our estimates showed that the $e^+e^-$ ratios were less than 0.04 for the HMS and less than $4.5 \cdot 10^{-4}$ for the SHMS. The background due to pions can easily be reduced below the 1% level using the calorimeters and Cerenkov counters of the spectrometers.

### 4.2 The Polarized Beam

In this proposal we shall assume that the achievable beam polarization at CEBAF is 80% with a current of $10\mu A$. The polarization of the beam will be measured with the Hall C Moller and Compton polarimeters. Both systems are expected to provide a minimum precision $\Delta P_b/P_b$ of 1.5%.

The impact of radiation and heat load on the target cells will be minimized by using the raster system to steer the beam through a circular pattern with a diameter appropriate to the target dimensions.

### 4.3 The Spectrometers

This proposal will make use of the base equipment proposed for the upgraded Hall C. Specifications for the SHMS and upgraded HMS have already been presented in Table 1. Pion rejection in the DIS region will be accomplished through the use of a gas Cerenkov and a lead-glass shower counter.

### 4.4 The Polarized $^3$He Target

The polarized $^3$He target at JLab is based on optical pumping of a vapor of alkali atoms and subsequent spin exchange between the polarized atoms and the $^3$He nuclei.

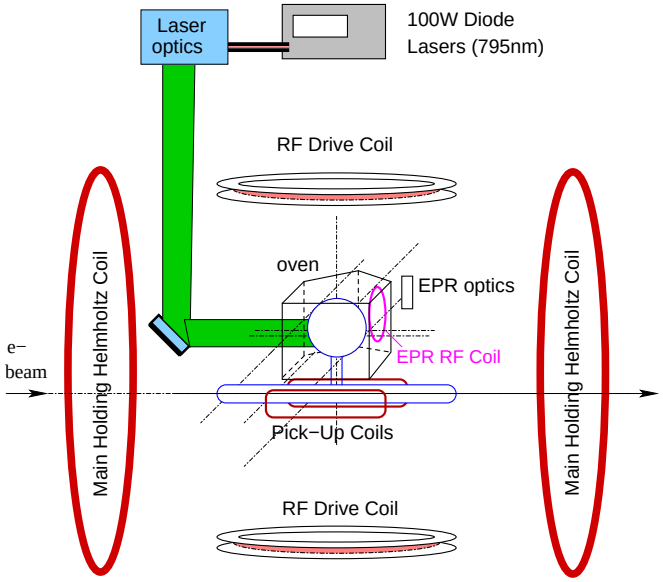


Figure 8: Typical layout of a polarized $^3$He target. Note that for simplicity, only one of the three sets of orthogonal Helmholtz coils shown.

Figure 8 shows the basic layout of the polarized $^3$He target which currently exists for research in Hall A [74]. The target holding field is provided by two sets of Helmholtz coils oriented normal to each other,

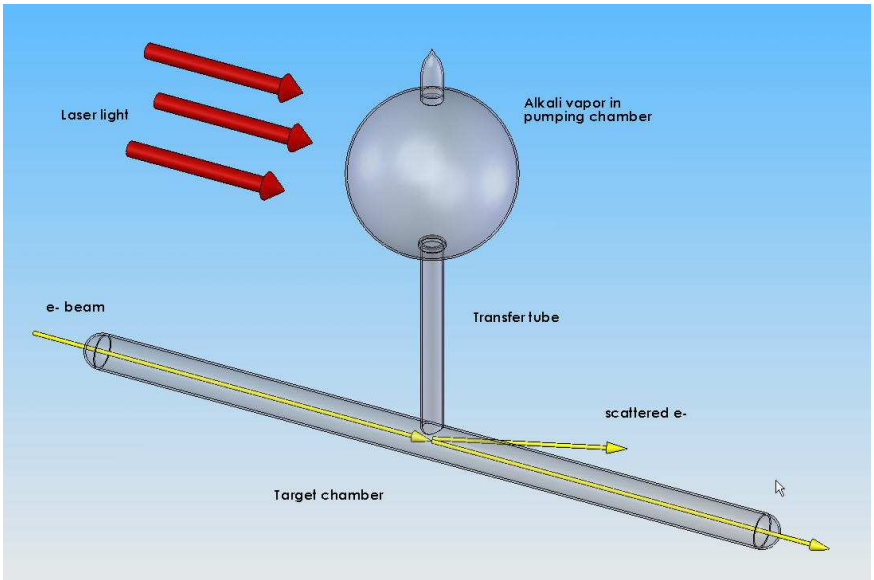


Figure 9: A standard polarized $^3$He target cell. The cell consists of a spherical "pumping chamber," a cylindrical "target chamber," and a "transfer tube" connecting the two chambers. The electron beam passes through the 40 cm long target chamber as shown.

hence the target spin direction can be aligned either parallel or perpendicular to the electron beam. Fig. 9 shows a picture of a standard 40 cm long cell. The cells for these experiments consist of a two chamber design. The upper spherical chamber contains the alkali vapor while the lower chamber is used for electron scattering from the polarized $^3$He.

Approximately 100 Watts (total) of light from a set of 3-4 diode lasers is combined using an optical fiber coupler and directed through a series of optics to produce circularly polarized light at a wavelength of $\sim 795$ nm. This light is used to polarized the alkali vapor through optical pumping. The polarized alkali transfers its spin to the $^3$He nuclei through collisions.

This target has been used by seven experiments in Hall A from 1998 to 2006 and is currently being re-designed for a series of five experiments planned for 2007 as shown in Figure 10. In addition to adding a third set of Helmholtz coils to allow for polarization in the vertical direction, the new system will incorporate new design features allowing it to capitalize on the recent success of a similar target used for experiment E02-013 [75]. So-called 'hybrid' target cells [76] containing a mixture of potassium and rubidium were used to achieve over 50% polarization with 8 $\mu$A of beam current. During E02-013 a single cell was used with a beam current of 8 $\mu$A for 6 weeks without rupturing. Beam currents up to 15 $\mu$A could be used with a degradation in polarization and cell lifetime.

The target polarization can be measured using two methods: NMR and EPR (Electron-Paramagnetic Resonance). Each type of polarimetry can provide a relative 3% precision. In this document we use a polarization of 50% to estimate the expected uncertainties and beam time request. With a beam current of 10 $\mu$A and a typical target density of 12 amg under operating conditions, this provides a $e-\vec{n}$ luminosity of $6.7 \times 10^{35}$ s$^{-1}$ cm$^{-2}$.

This target continues to be a flagship facility for the Hall A program and will be relatively easy to adapt for use at 11 GeV in Halls A and C. Polarized target groups at the College of William and Mary and the University of Virginia continue to produce target cells with consistently-improving polarization. Through the combined effort of these groups and the polarized target groups and personnel at the University of Kentucky, Temple University, Duke University and Jefferson Lab this collaboration has the necessary

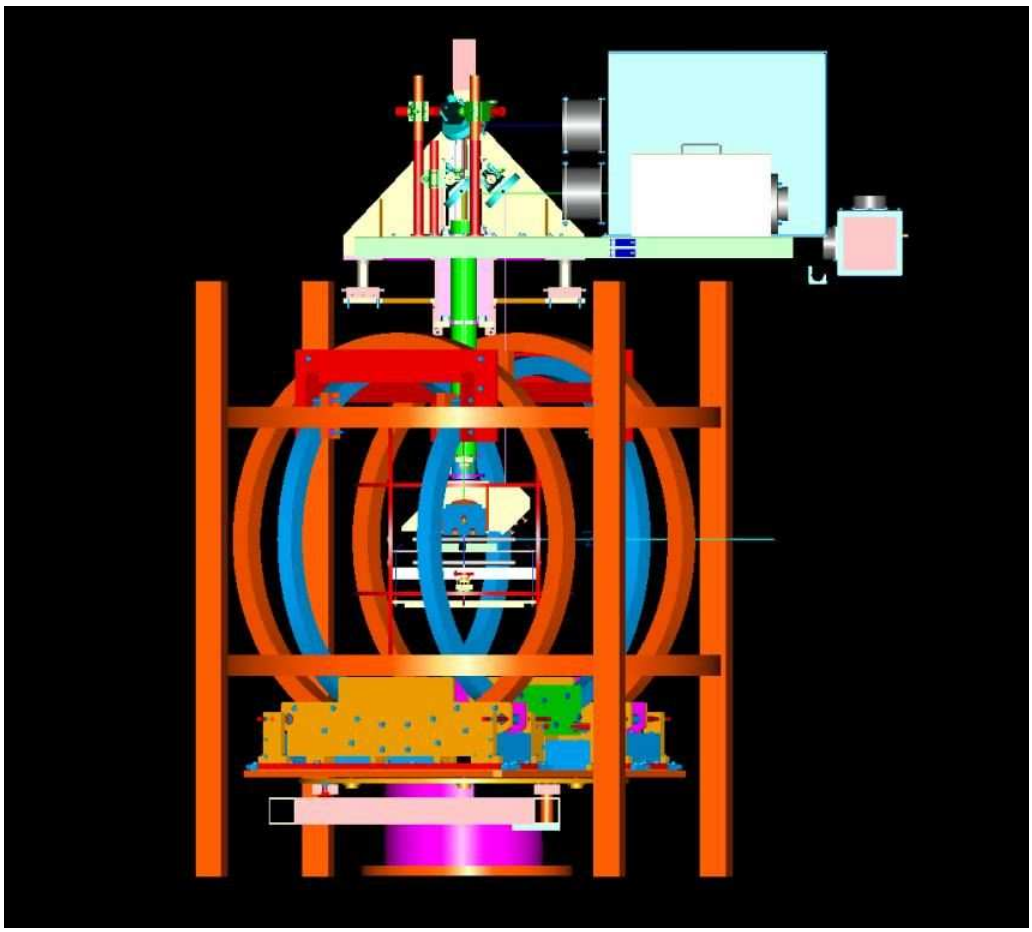

Figure 10: Current design (side view) of the Hall A polarized target system for the series of experiments planned for 2007-08. It is expected that this target system can be used with little modification for the 11 GeV programs in Halls A and C. Though the target itself is well-suited for use in Hall A or C, a new mounting system at the pivot, and accommodations for the lasers, will be needed for use in Hall C.

experience and manpower for this polarized target system.

# 5 Corrections and systematic uncertainties for $g_2^n$ and $d_2^n$

## 5.1 Radiative Corrections

The radiative corrections (RC) will be performed in two stages. First, the internal corrections will be evaluated following the procedure developed by Bardin and Shumeiko[45] for the unpolarized case and extended to the spin dependent lepto-production cross sections by Akushevish and Shumeiko[57, 58]. Second, using these internally corrected cross sections, the external corrections (for thick targets) are applied by extending the procedure developed for the unpolarized cross sections by Tsai[59, 60] with modifications appropriate for this experiment.

The present measurement is self sufficient to provide input data for the iterative unfolding procedure used in the radiative corrections of these same data, except for the lowest momentum transfer region. However previous measurements at JLab at 6 GeV provide for the remaining input data to complete this process with no need for input models. This is important since we are interested in providing for helicity dependent cross sections not only in the deep inelastic region where world fits of structure functions are available but also the resonance region where modeling is still tentative especially for a nucleus like $^3$He.

## 5.2 Spin Structure Functions: From $^3$He to the Neutron

Because the deuteron polarization is shared roughly equally between the proton and neutron, extraction of neutron spin structure functions requires a precise knowledge of the proton spin structure, in addition to the nuclear effects [62]. This problem is compounded by the fact that the spin-dependent structure functions of the proton are typically much larger than those of the neutron, making extraction of the latter especially sensitive to small uncertainties in the proton structure functions. In $^3$He, however, the neutron carries almost 90% of the nuclear spin making polarized $^3$He an ideal source of polarized neutrons.

The three-nucleon system has been studied for many years, and modern three-body wave functions have been tested against a large array of observables which put rather strong constraints on the nuclear models [63]. In particular, over the past decade considerable experience has been acquired in the application of three-body wave functions to deep-inelastic scattering [64, 65, 66].

The conventional approach employed in calculating nuclear structure functions in the region $0.3 < x < 0.8$ is the impulse approximation, in which the virtual photon scatters incoherently from individual nucleons in the nucleus [67]. Corrections due to multiple scattering, $NN$ correlations or multi-quark effects are usually confined to either the small-$x$ ($x < 0.2$), or very large-$x$ ($x > 0.9$) regions. In the impulse approximation the $g_1$ structure function of $^3$He, in the Björken limit ($Q^2, \nu \to \infty$), is obtained by folding the nucleon structure function with the nucleon momentum distribution $\Delta f_N$ ($N = p, n$) in $^3$He:

$$g_1^{^3\mathrm{He}}(x) \;=\; \int_x^3 \frac{dy}{y}\,\left\{2\Delta f_p(y)\; g_1^p(x/y) \;+\Delta f_n(y)\; g_1^n(x/y)\right\}, \tag{17}$$

where $y$ is the fraction of the $^3$He momentum carried by the nucleon, and the dependence on the scale, $Q^2$, has been suppressed. The nucleon momentum distributions $\Delta f_N(y)$ are calculated from the three-body nuclear wave function, which are obtained by either solving the Faddeev equation [68] or using variational methods [65], and are normalized such that:

$$\int_0^3 dy\,\Delta f_N(y) \;=\; \rho_N\,, \tag{18}$$

where $\rho_N$ is the polarization of the nucleon in $^3$He. While the full three-body wave function involves summing over many channels, in practice the three lowest states, namely the $S$, $S'$ and $D$, account for over 99% of the normalization. Typically, one finds $\rho_n \approx 87\%$ and $\rho_p \approx -2\%$ [63, 64, 65, 66, 68].

The smearing in Eqn.(17) incorporates the effects of Fermi motion and nuclear binding. Correctly accounting for these effects is important when attempting to extract information on nucleon structure functions from nuclear data at $x > 0.6$, as well as for determining higher moments of structure functions, in which the large-$x$ region is more strongly weighted.

The nuclear corrections to the $g_2^n$ structure function can be evaluated analogously to those for $g_1^n$. One can estimate the order of magnitude of the effects by considering firstly the twist-2 part of $g_2^n$, which is determined from $g_1^n$ through the Wandzura-Wilczek relation [42, 70]:

$$g_2^{^3\mathrm{He}}(x)\Big|_{\mathrm{tw-2}} \;=\; -g_1^{^3\mathrm{He}}(x) \;+\; \int_x^3 \frac{dy}{y}\, g_1^{^3\mathrm{He}}(x/y)\;, \tag{19}$$

where $g_1^{^3\mathrm{He}}$ is given by Eqn.(17). The main effect numerically at moderate to large $x$ is due to the difference between the neutron and $^3$He polarizations, as the effects due to smearing peaks at the level of a few percent at $x \sim 0.6$. Similarly, the difference in the second moments of $g_2^{^3\mathrm{He}}$ between the convolution results using different $^3$He wave functions is a few percent [68,69]. Moreover, since the main objective of the experiment is to extract the second moment of $3g_2^n + 2g_1^n$, namely $\int dx\, x^2(3g_2^n(x) + 2g_1^n(x))$, the sensitivity of the correction to $x$ variations of the integrand is reduced compared to a direct extraction of the $g_2$ or $g_1$ structure functions themselves. degli Atti [65] showed that nuclear binding effects are quite sizable for $g_1^n$ in the resonance region at $Q^2$ values of $1\,\mathrm{GeV}^2/c^2$ when extracted from polarized $^3$He. However, the nuclear effects are small $< 4\%$ in the DIS region ($Q^2 = 10\,\mathrm{GeV}^2/c^2$). Our own data, taken during the Bloom-Gilman duality experiment (E01-012), show that the resonance structures disappear for $Q^2$ $/gtrsim\, 3\,\mathrm{GeV}^2/c^2$.

While the nuclear model dependence of the nuclear correction appears to be relatively weak for the twist-2 approximation in the Björken limit, an important question for the kinematics relevant to this experiment is how are these effects likely to be modified at finite $Q^2$? To address this question one needs to obtain generalizations of Eqns. (17) and (19) which are valid at any $Q^2$, and which can incorporate the twist-3 component of $g_2$. In fact, at finite $Q^2$ one finds contributions from $g_1^N$ to $g_2^{^3\mathrm{He}}$, and from $g_2^N$ to $g_1^{^3\mathrm{He}}$. The latter vanish in the Björken limit, but the former are finite, although they depend on the Fermi momentum of the bound nucleons. These corrections can be calculated by working directly in terms of the (unintegrated) spectral function $S(\vec{p},E)$, where $p$ is the bound nucleon momentum and $E$ is the separation energy, rather than in terms of the momentum distribution functions $\Delta f_N(y)$. Following Schulze & Sauer [66], it is convenient to parametrize the $^3$He spectral function according to:

$$S(\vec{p},E) \;=\; \frac{1}{2}\left( f_0 + f_1 \vec{\sigma}_N\cdot\vec{\sigma}_A + f_2\left[\vec{\sigma}_N\cdot\hat{p}\;\vec{\sigma}_A\cdot\hat{p} \;-\frac{1}{3}\vec{\sigma}_N\cdot\vec{\sigma}_A\right]\right)\;, \tag{20}$$

where $\vec{\sigma}_N$ and $\vec{\sigma}_A$ are the spin operators of the nucleon and $^3$He, respectively, and the functions $f_{0,1,2}$ are scalar functions of $|\vec{p}|$ and $E$. The function $f_0$ contributes to unpolarized scattering only, while $f_1$ and $f_2$ determine the spin-dependent structure functions. In terms of these functions, at finite $Q^2$ one has a set of

coupled equations for $g_1^{^3\mathrm{He}}$ and $g_2^{^3\mathrm{He}}$ [72]:

$$
\begin{aligned}
& x g_1^{^3\mathrm{He}}(x,Q^2) + (1-\gamma^2) x g_2^{^3\mathrm{He}}(x,Q^2) \\
= & \sum_{N=p,n} \int d^3p\, dE\, (1-\frac{\varepsilon}{M}) \left\{ \left[ \left( 1 + \frac{\gamma p_z}{M} + \frac{p_z^2}{M^2} \right) f_1 + \left( -\frac{1}{3} + \hat{p}_z^2 + \frac{2\gamma p_z}{3M} + \frac{2p_z^2}{3M^2} \right) f_2 \right] z g_1^N(z,Q^2) \right. \\
& \left. + (1-\gamma^2)(1 + \frac{\varepsilon}{M} \left[ f_1 + \left( \frac{p_z^2}{\vec{p}^2} - \frac{1}{3} \right) f_2 \right] \frac{z^2}{x} g_2^N(z,Q^2) \right\} , \qquad (21)
\end{aligned}
$$

$$
\begin{aligned}
& x g_1^{^3\mathrm{He}}(x,Q^2) + x g_2^{^3\mathrm{He}}(x,Q^2) \\
= & \sum_{N=p,n} \int d^3p\, dE\, (1-\frac{\varepsilon}{M}) \left\{ \left[ \left( 1 + \frac{p_x^2}{M^2} \right) f_1 + \left( \vec{p}_x^2 - \frac{1}{3} + \frac{2p_x^2}{3M^2} \right) f_2 \right] z g_1^N(z,Q^2) \right. \\
& \left. + \left[ \left( 1 + \frac{p_x^2}{M^2}(1-z/x) \right) f_1 + \left( \vec{p}_x^2 - \frac{1}{3} + \frac{2p_x^2}{3M^2}(1-z/x) - \frac{\gamma p_z \hat{p}_x^2}{M} \frac{z}{x} \right) f_2 \right] z g_2^N(z,Q^2) \right\} , \qquad (22)
\end{aligned}
$$

with $\gamma = \sqrt{1+4M^2x^2/Q^2}$ a kinematic factor parametrizing the finite $Q^2$ correction, $\varepsilon \equiv \vec{p}^2/4M - E$, and $z = x/(1+(\varepsilon+\gamma p_z)/M)$. Equations (21) and (22) can then be solved to obtain $g_1^{^3\mathrm{He}}$ and $g_2^{^3\mathrm{He}}$ explicitly. For $Q^2 \to \infty$ Eqns. (21) and (22) reduce to simple one-dimensional convolution expressions, as in Eqn. (17). At finite $Q^2$, however, the smearing function effectively becomes $x$ and $Q^2$ dependent, so that the amount of smearing in general will depend on the shape of the nucleon structure functions.

The nuclear correction of most interest for this experiment is that to the $g_2$ structure function. One can test the sensitivity to the kinematic $Q^2$ dependence, as distinct from the $Q^2$ dependence in the nucleon structure function itself, by taking the same input neutron structure function for all values of $Q^2$ at which $x g_2^{^3\mathrm{He}}$ is evaluated. One finds [72] that the effect of the kinematic $Q^2$ dependence turns out to be rather small at $Q^2 \sim$ 1–4 GeV$^2$, and only becomes noticeable for low $Q^2 \sim 0.2$ GeV$^2$. Furthermore, at these values of $Q^2$ the $g_1^n$ contribution to $g_2^{^3\mathrm{He}}$ is negligible compared with the lowest order neutron polarization correction. This confirms earlier analyses of the nuclear corrections by the Rome-Perugia group [73].

There was also an investigation in Ref. [71] into the role of the $\Delta(1232)$ in deep-inelastic scattering on polarized $^3$He and its effects on the $g_1$ neutron spin structure function extraction. The authors estimated that when taking the effect of the $\Delta$ into account the values of the first moment of $g_1^n$ increases by 6—8 %.

In summary, all of the nuclear structure function analyses that have been performed suggest that both the neutron $g_1^n$ and $g_2^n$ structure functions can be extracted from $^3$He data with minimal uncertainties associated with nuclear corrections. Estimating all the corrections and their uncertainties we come to the conclusion that in this experiment the statistical error on the final result is still the dominant error.

### 5.3 Target Spin Misalignment

One item of concern was the effect of the target relative spin misalignment between the transverse and longitudinal direction measurements. Fig. 11 shows this effect at each value of $x$ on the integrand of $d_2$. Calculations assuming a relative error of $0.5^\circ$ in the relative direction of the transverse versus perpendicular results in a relative error $\Delta d_2/d_2 = 0.15\%$. Using the Weigel *et al.* [61] model of $g_2$ and $g_1$ we estimated $\Delta d_2/d_2$ to be of the order of 10 % and thus an absolute systematic uncertainty of about $1.5 \cdot 10^{-3}$. Recent implementation of a precision air compass (used during $G_{E_n}$ in Hall A) have reduced the uncertainty in the target spin alignment measurement to better than $0.1^\circ$ suggesting a more realistic (but still conservative) estimate would be $< 5 \times 10^{-4}$.

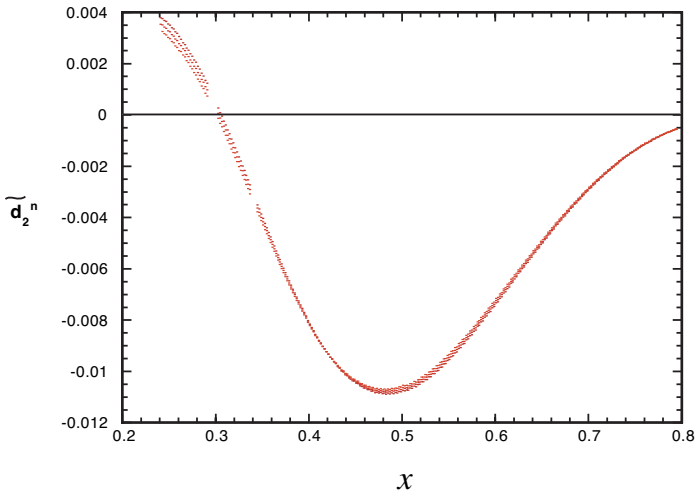


Figure 11: Effect of target relative spin misalignment by 0.5° between the transverse and longitudinal measurements

## 5.4 Summary of Systematic Uncertainties

To evaluate the remaining experimental systematic uncertainties for $g_2^n$ and $d_2^n$ we used relative uncertainties in the cross sections and asymmetries achieved in JLab E94-010, E97-103 and E99-117. Table 5.4 summarizes these estimates.

With our improved projected statistical precision the total uncertainty in the measured quantities will be almost equally shared between the statistical and the systematic accuracy of the measurement.

An elastic scattering asymmetry measurement is planned at low energy ($E_i$ = 2.2 GeV) with both the SHMS and the HMS spectrometers at $\theta = 12.5^\circ$ to calibrate our spin dependent absolute cross sections. This quantity can be evaluated using the measured electric and magnetic form factors of $^3$He. This measurement would actually determine the polarization of the $^3$He nuclei along the electron beam path. False asymmetries will be checked to be consistent with zero by comparing data with target spins in opposite directions.

Also contributing to the dilution of the asymmetry is the pair-electron contamination. This correction is $x$ dependent, and is relevant only in the low $x$ region. This contamination was estimated to be no more than 6% in the worst case and will be measured in this experiment by reversing the spectrometer polarity on the HMS and SHMS spectrometers.

Table 4: List of the systematic error contributions to $g_2^n$ and $d_2^n$

| Item description | Subitem description | Relative uncertainty |
|---|---|---|
| **Target polarization** | | 1.5 % |
| **Beam polarization** | | 3 % |
| **Asymmetry (raw)** | | |
| | • Target spin direction ($0.1^\circ$) | $< 5 \times 10^{-4}$ |
| | • Beam charge asymmetry | $< 50$ ppm |
| **Cross section (raw)** | | |
| | • PID efficiency | $< 1$ % |
| | • Background Rejection efficiency | $\approx 1$ % |
| | • Beam charge | $<$ 1 % |
| | • Beam position | $<$ 1 % |
| | • Acceptance cut | 2-3 % |
| | • Target density | $< 2$% |
| | • Nitrogen dilution | $< 1$% |
| | • Dead time | $<$1% |
| | • Finite Acceptance cut | $<$1% |
| **Radiative corrections** | | $\leq 5$ % |
| **From $^3$He to Neutron correction** | | 5 % |
| **Total systematic uncertainty (for both $g_2^n(x,Q^2)$ and $d_2(Q^2)$)** | | $\leq 10$ % |
| **Estimate of contributions to $d_2$ from unmeasured region** | $\int_{0.003}^{0.23} \tilde{d}_2^n \, dx$ | $4.8 \times 10^{-4}$ |
| **Projected absolute statistical uncertainty on $d_2$** | | $\Delta d_2 \approx 5 \times 10^{-4}$ |
| **Projected absolute systematic uncertainty on $d_2$ (*assuming* $d_2 = 5 \times 10^{-3}$)** | | $\Delta d_2 \approx 5 \times 10^{-4}$ |

# 6 Summary

## 6.1 The Proposal in Hall C

In summary, we request 700 hours (29 days) of beam to measure the unpolarized cross section $\sigma_0^{^3He}$, the parallel asymmetry $A_\parallel^{^3He}$ and the perpendicular asymmetry $A_\perp^{^3He}$. The request involves 200 hours each for three groups of SHMS/HMS kinematics plus an additional 100 hours for calibration and overhead.

Those data will be used to extract the $g_2^n$ structure function on the neutron over the extensive kinematic region $0.2 < x < 0.95$ and $2.5 < Q^2 < 6\text{GeV}^2/c^2$. In addition to mapping out the $x$ and $Q^2$ evolution of $g_2^n$ which (in contrast to $g_1$) is poorly understood at high $x$, we will extract the higher twist piece of the spin structure function $\bar{g}_2$ and evaluate the quantity $d_2^n = \int_0^1 \bar{g}_2\, dx = \int_0^1 x^2(2g_1 + 3g_2)\, dx$ at *constant* $Q^2$ for the very first time for $Q^2 > 1\ \text{GeV}^2/c^2$. All previous measurements of $d_2^n$ at higher $Q^2$ have required data taken over a broad range of $Q^2$ values to be evolved to some common $Q^2$ prior to evaluating the $d_2$ integral. At higher $x$, this evolution has required the transform from $Q^2$'s of as much as $15\,\text{GeV}^2/c^2$ down to $5\,\text{GeV}^2/c^2$. Figure 12 shows the $(x, Q^2)$ coverage for this proposal. Figure 13 presents the estimated statistical errors associated with the extracted $x^2 g_2^n$ values against the present world data.

The upgraded SHMS/HMS combination in Hall C at Jefferson Lab provides an ideal environment for this measurement. The large momentum acceptance of the SHMS allows a very broad $x$ region to be measured over nearly constant $Q^2$ in a single kinematic setting. The HMS can then be used to simultaneously fill in gaps in the low-$x$ region, resulting in nearly contiguous $x$ coverage over a broad $Q^2$ band – something that has never before been accomplished. The combined data will allow the extraction of $d_2^n(Q^2)$ at truly constant $Q^2$'s of 3, 4, and $5\,\text{GeV}^2/c^2$. The precision with which these values may be measured, combined with explicit information on the $Q^2$ evolution of $d_2$ provide a strict test of Lattice QCD.

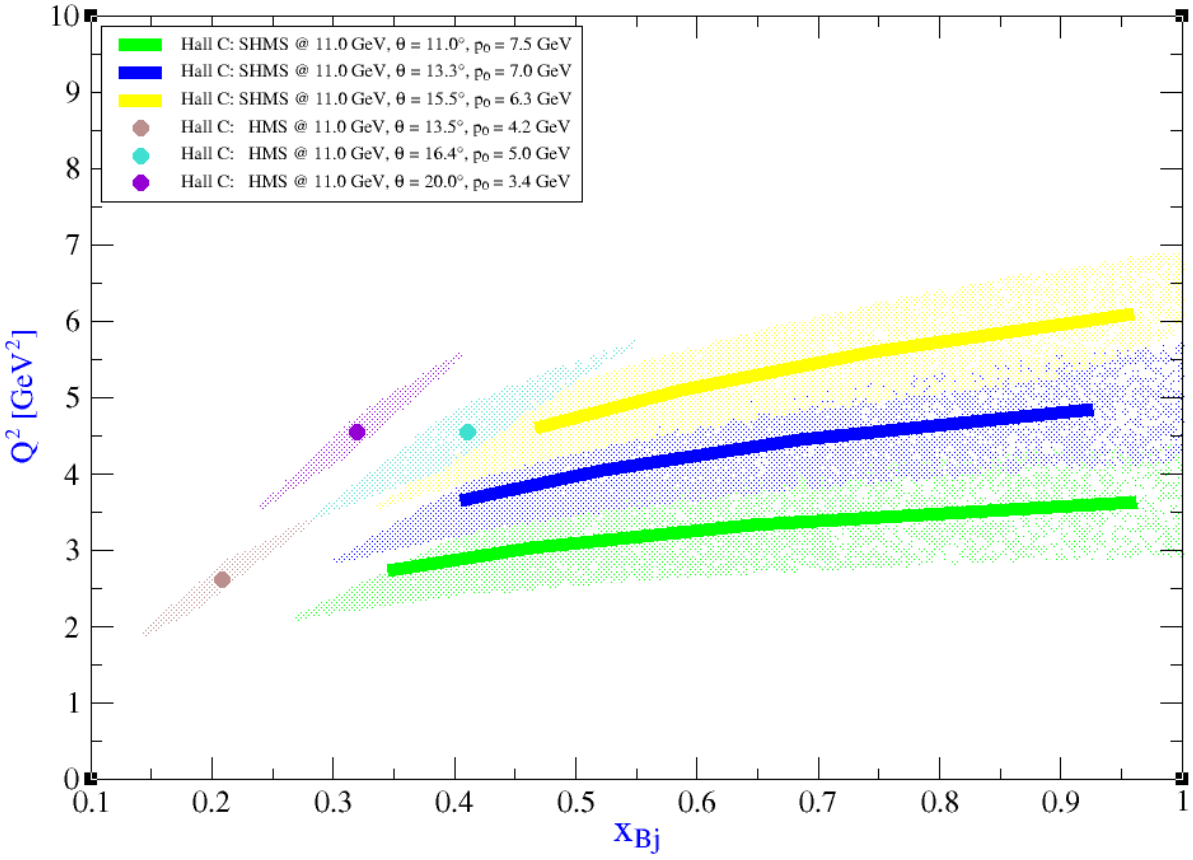


Figure 12: Kinematic coverage for the six kinematic settings for the proposed experiment. The three SHMS bands will be subdivided into four bins each during offline analysis. The lower stripes reflect the coverage from the lower energy measurement E06-014.

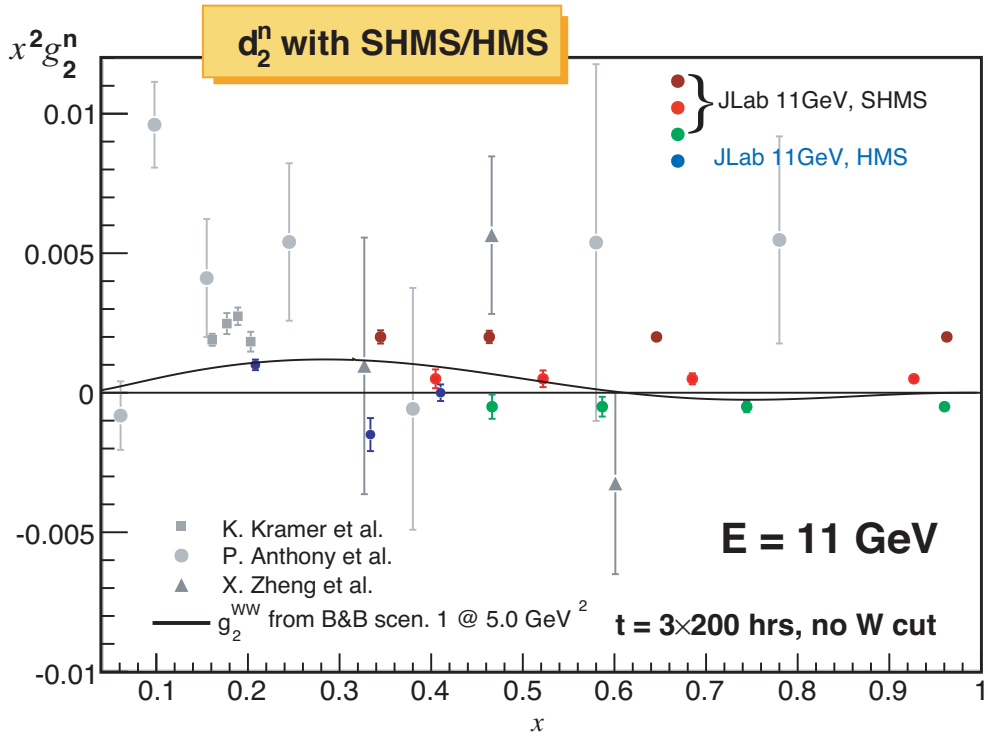


Figure 13: $x^2 g_2^n(x)$ *vs.* $x$ presenting the statistical errors expected from the proposed measurement (colored circles). Existing world data are also shown. **Note:** The points associated with the present measurement are distributed along different horizontal lines, each representing a common $< Q^2 >$ value. This is in marked contrast to the existing world data for $g_2^n$ for $Q^2 > 1\,\mathrm{GeV}^2/c^2$ which were measured over $Q^2$ values ranging from 1—15 $\mathrm{GeV}^2/c^2$ and were "evolved" to a common $Q^2$ prior to computing $d_2$.

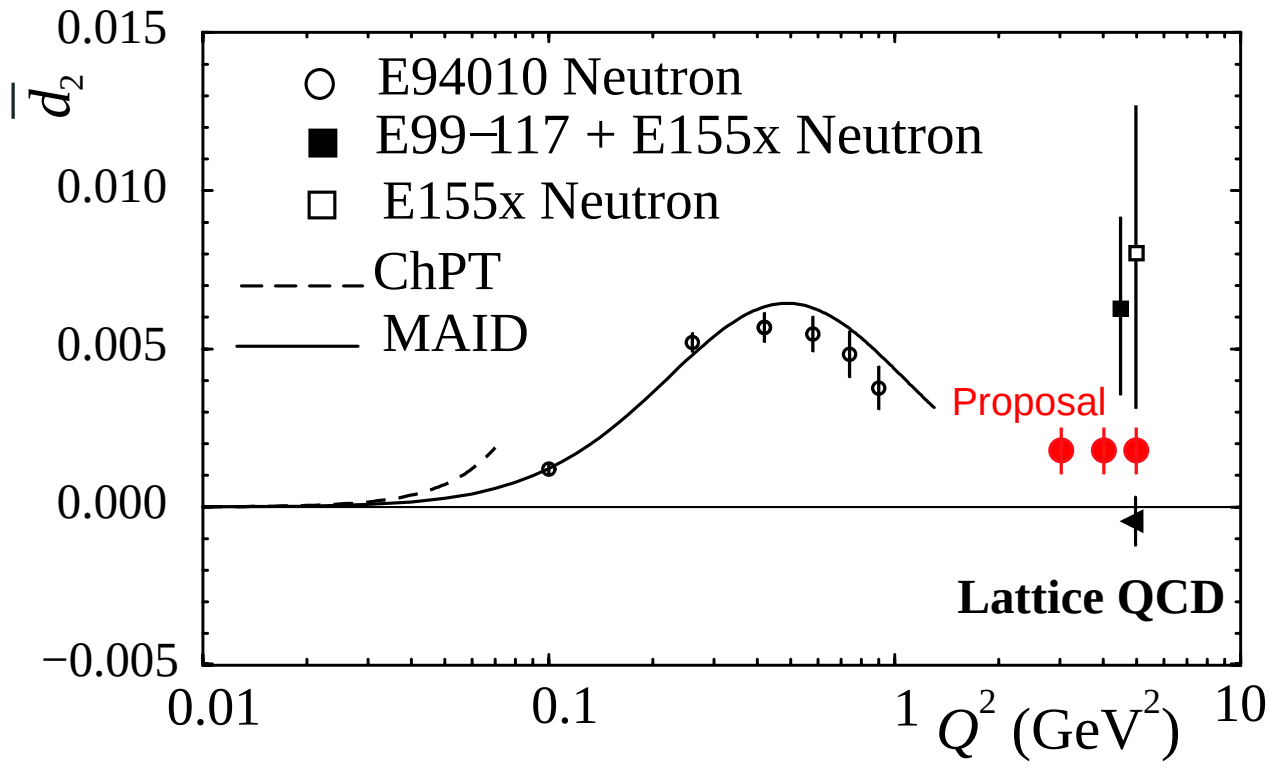


Figure 14: $\bar{d}_2(Q^2)$ without the nucleon elastic contribution are presented with estimated statistical errors for the proposed measurement. The SLAC E155 [38] neutron result is also shown here (open square). The solid line is the MAID calculation[55] while the dashed line is a HB$\chi$PT calculation[56] valid only at very low $Q^2$. The lattice prediction [51] at $Q^2$ = 5 GeV$^2$ for the neutron $d_2$ reduced matrix element is negative but consistent with zero. We note that all models shown in Fig. 3 predict a negative value or zero at large $Q^2$ where the elastic contribution is negligible. At moderate $Q^2$ the data show a positive $\bar{d}_2^n$, and indicate a slow decrease with $Q^2$. The combined SLAC+JLab datum shows a positive $d_2^n$ value but with still a large error bar.

## 6.2 The *Complementary* Proposal in Hall A

We would also like to comment on a "sister" proposal for Hall A (also requesting 700 hours) that has also been submitted to the PAC30 board. The kinematic coverage of the Hall A measurement was been specifically selected to compliment the coverage of the Hall C proposal. BigBite in Hall A is ideally suited to map out the the high-$x$, high-$Q^2$ region with excellent statistics in a modest time. In contrast, the SHMS/HMS in Hall C is uniquely suited to make a *definitive* measurement of the $Q^2$ evolution of $d_2^n$ in the central $Q^2$ range due to its uniquely flat $Q^2$ coverage per bin over $0.4 < x < 1$. This allows $d_2$ to be explicitly evaluated at several $Q^2$ values *without* evolving the integrand. An open geometry detector like BigBite is not able to match such kinematics due to rate limitations at forward angles. Figure 15 shows the combined coverage of the pair of proposed measurement in Halls A and C and highlights proposed lines of integration for $d_2$ and regions of study for the $Q^2$ evolution of $g_2$. The information that could be extracted from such a combined effort is truly impressive.

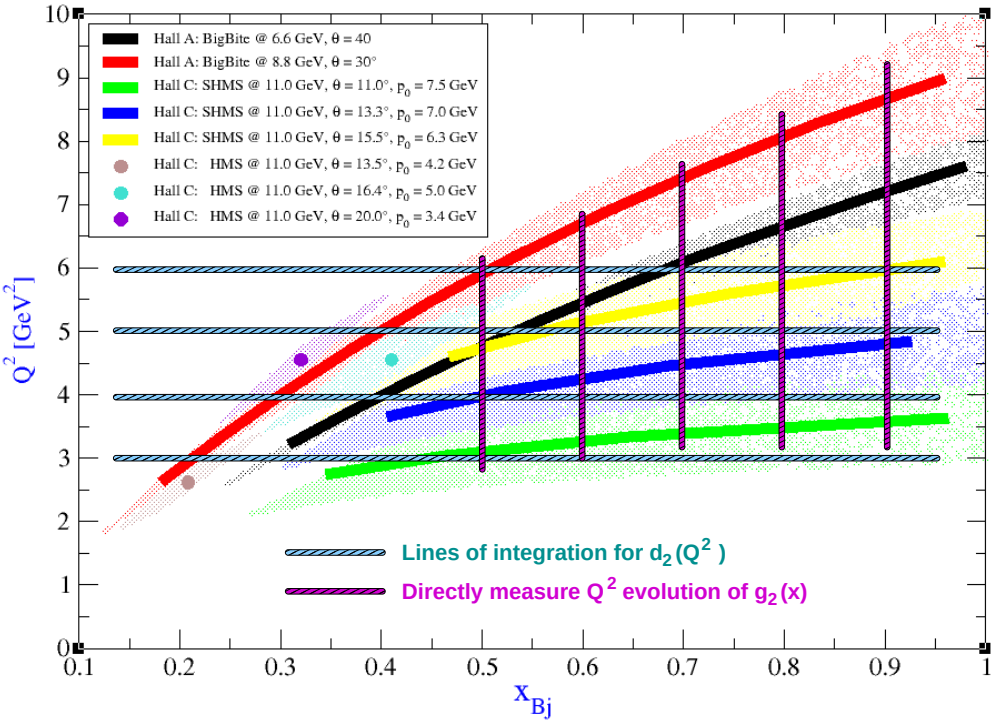


Figure 15: The combined kinematic coverage for the pair of complimentary experiments proposed in Halls A and C. In addition to simply mapping out $g_2(x, Q^2)$ over a very broad range of $x$ and $Q^2$, the vertical lines show the $x$ values where a thorough $Q^2$ evolution study can be accomplished. The horizontal lines show how the combined data could be binned to compute $d_2^n(Q^2)$ at almost constant $Q^2$ for a broad range of $Q^2$.

# 7 Bibliography

## References


[1] A.D. Martin, R.G. Roberts, W.J. Stirling, R.S. Thorne; hep-ph/0201127.

[2] J. Pumplin et al.; hep-ph/0303013.

[3] H1 Collaboration; C. Adloff et al., Eur. Phys. J. C30, 1 (2003).

[4] P. Bosted, CLAS-NOTE-2004-005.

[5] D.E. Wiser, Ph.D. thesis, Univ. of Wisconsin (1977).

[6] E. Shuryak and A. Vainshtein, Nuc. Phys. B **201** (1982) 141.

[7] R. L. Jaffe and X. Ji, Phys. Rev. D **43** (1991) 724.

[8] B. W. Filippone and X. Ji, Adv. in Nucl. Phys. **26**, 1 (2001).

[9] S. Wandzura and F. Wilczek, Phys. Lett. B **72**, 195 (1977).

[10] E. Stein, P. Gornicki, L. Mankiewicz and A. Schäfer, Phys. Lett. B 353, 107 (1995).

[11] X. Ji, arXiv:hep-ph/9510362.

[12] X. Ji and P. Unrau, Phys. Lett. B **333** (1994) 228.

[13] X. Ji Nucl. Phys. **B402** (1993) 217.

[14] S. A. Larin, T. van Ritbergen and J.A. Vermaseren, Phys. Lett. **404**, 153 (1997); S. A. Larin, Phys. Lett. B **334**, 192 (1994).

[15] F. E. Close and R. G. Roberts, Phys. Lett. B **336**, 257 (1994).

[16] X. Ji and W. Melnitchouk, Phys. Rev. D **56**, 1 (1997).

[17] J. Edelmann, G. Piller, W. Weise, N. Kaiser, Nucl. Phys. A **665** (2000) 125.

[18] S. Simula, M. Osipenko, G. Ricco and M. Tauiti, hep/0205118 and references therein.

[19] M. Osipenko *et al.*, Phys. Lett. B **609**, 259 (2005) [arXiv:hep-ph/0404195].

[20] Z. E. Meziani *et al.*, Phys. Lett. B **613**, 148 (2005) [arXiv:hep-ph/0404066].

[21] A. Deur *et al.*, Phys. Rev. Lett. **93**, 212001 (2004) [arXiv:hep-ex/0407007].

[22] A. V. Sidorov and C. Weiss, Phys. Rev. D **73**, 074016 (2006) [arXiv:hep-ph/0602142].

[23] X. Ji, in Proceeding of the Workshop on Deep Inelastic scattering and QCD, Editors: JF. Laporte et Y. Sirois Paris, France, 24-28 April, 1995 (ISBN 2-7302-0341-4).

[24] P. L. Anthony *et al.* [E155 Collaboration], Phys. Lett. B **458**, 529 (1999) [arXiv:hep-ex/9901006].

[25] H. Burkhardt and W. N. Cottingham, Ann. Phys. **56** (1970) 453.

[26] R. Jaffe, Comments Nucl. Part. Phys. 19 (1990) 239.

[27] I. P. Ivanov *et al.*, Phys. Rep. **320**, 175 (1999).

[28] M. Anselmino, A. Efremov and E. Leader, Phys. Rep. **261**, 1 (1995).

[29] G. Altarelli, B. Lampe, P. Nason and G. Ridolfi, Phys. Lett. B **334**, 187 (1994).

[30] M. Amarian *et al.*, Phys. Rev. Lett. **89**, 242301 (2002).

[31] M. Amarian *et al.*, Phys. Rev. Lett. **92**, 022301 (2004).

[32] D. Adams *et al.*, Phys. Lett. **B336** (1994) 125.

[33] P. L. Anthony *et al.*, Phys. Rev. Lett. **71** (1993) 959.

[34] P. L. Anthony *et al.*, Phys. Rev. D **54** (1996) 6620.

[35] K. Abe *et al.*, Phys. Rev. Lett. **76** (1996) 587.

[36] K. Abe *et al.*, Phys. Lett. B **404** (1997) 377.

[37] P. L. Anthony *et al.*, Phys. Lett. B**458** (1999) 529.

[38] P. L. Anthony *et al.* [E155x Collaboration], Phys. Lett. B **553**, 18 (2003) [arXiv:hep-ex/0204028].

[39] X. Zheng *et al.* [Jefferson Lab Hall A Collaboration], Phys. Rev. C **70**, 065207 (2004) [arXiv:nucl-ex/0405006].

[40] K. Kramer *et al.*, Phys. Rev. Lett. **95**, 142002 (2005) [arXiv:nucl-ex/0506005].

[41] K. Abe *et al.*, Phys. Rev. D **58** (1998) 112003-1.

[42] S. Wandzura and F. Wilczek, Phys. Lett. B **72** (1977) 195.

[43] JLab E01-012 experiment, Spokespeople N. Liyanage, J. P. Chen and Seonho Choi.

[44] JLab E01-006 experiment, Spokesperson O. Rondon and M. Jones

[45] D. Yu. Bardin and N. M. Shumeiko, Nucl. Phys. B **127** (1977) 1251.

[46] M. Wakamatsu, Phys. Lett B **487** (2000) 118.

[47] M. Stratmann, Z. Phys. C **60** (1993) 763.

[48] E. Stein, Phys. Lett. B **343** (1995) 369.

[49] B. Ehrnsperger, A Schäfer, Phys. Rev. D **52** (1995) 2709.

[50] I. Balitsky, V. Barun, A. Kolesnichenko, Phys. Lett. B **242** (1990) 245; B **318** (1995) 648 (E).

[51] M. Gockeler *et al.*, Phys. Rev. D **72**, 054507 (2005) [arXiv:hep-lat/0506017].

[52] M. Gockeler *et al.*, Phys. Rev. D **63**, 074506 (2001), [hep-lat/0011091].

[53] R. G. Edwards *et al.* [LHPC Collaboration], Private communication

[54] C. R. V. Bourrely, J. Soffer and F. Buccella, Eur. Phys. J. C **41**, 327 (2005) [arXiv:hep-ph/0502180].

[55] D. Drechsel, S. Kamalov and L. Tiator, Phys. Rev. D **63**, 114010 (2001).

[56] C. W. Kao, T. Spitzenberg and M. Vanderhaeghen, Phys. Rev. D **67**, 016001 (2003).

[57] T.V. Kuchto and N. M. Shumeiko, Nucl. Phys. B **219** (1983) 412.

[58] I. V. Akushevich and N. M. Shumeiko, J. Phys. **G**: Nucl. Part. Phys. **20** (1994) 513.

[59] L. W. Mo and Y. S. Tsai, Rev. Mod. Phys. **41** (1969) 205.

[60] Y. S. Tsai, SLAC-PUB-848 (1971).

[61] H. Weigel, L. Gamberg, H. Reinhart, Phys. Rev. D**55** (1997) 6910.

[62] W. Melnitchouk, G. Piller and A.W. Thomas, Phys. Lett. B **346** (1995) 165; S. A Kulagin, W. Melnitchouk, G. Piller and W. Weise Phys. Rev. C **52** (1995) 932.

[63] J.L. Friar et al., Phys. Rev. C **42** (1990) 2310.

[64] R.M. Woloshyn, Nucl. Phys. A **496** (1989) 749.

[65] C. Ciofi degli Atti, E. Pace and G. Salme, Phys. Rev. C **46** (1992) R1591; C. Ciofi degli Atti, S. Scopetta, E. Pace, G. Salme, Phys. Rev. C **48** (1993) 968;

[66] R.W. Schulze and P.U. Sauer, Phys. Rev. C **48** (1993) 38.

[67] D.F. Geesaman, K. Saito and A.W. Thomas, Ann. Rev. Nucl. Part. Sci. **45** (1995) 337.

[68] I.R. Afnan, F. Bissey and A.W. Thomas, Phys. Rev. C**64** (2001) 024004.

[69] I.R. Afnan, F. Bissey, J. Gomez, A.T. Katramatou, W. Melnitchouk, G.G. Petratos and A.W. Thomas, Phys. Lett. B **493** (2000) 36.

[70] F. Bissey, W. Melnitchouk, A. W. Thomas, in preparation.

[71] C. Boros, V. Guzey, M. Strikman, A.W. Thomas, Phys. Rev. **D64** (2001) 014025 and hep-ph/0008064.

[72] S.A. Kulagin and W. Melnitchouk, in preparation.

[73] S. Scopetta, private communication.

[74] J. Alcorn *et al.*, Nucl. Inst. Meth. A **522** (2004) 294.

[75] G. Cates *et al.*, Jefferson Lab E02-013 Proposal, http://www.jlab.org/exp_prog/proposals/02/PR02-013.pdf.

[76] E. Babcock *et al.*, Phys. Rev. Lett. **91** (2003) 123003.